Ecological Informatics 81 (2024) 102632

Contents lists available at ScienceDirect

Ecological Informatics

journal homepage: www.elsevier.com/locate/ecolinf

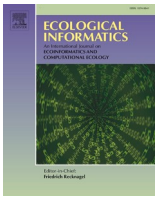

Evaluating error sources to improve precision in the co-registration of underwater 3D models

Marine A.A. Lechene [a,b,*], Will F. Figueira [c], Nicholas J. Murray [a], Eoghan A. Aston [a,b], Sophie E. Gordon [b], Renata Ferrari [b]

[a] College of Science and Engineering, James Cook University, 1 James Cook Dr, Douglas, QLD 4811, Australia
[b] Australian Institute of Marine Science, Townsville, QLD 4810, Australia
[c] School of Life and Environmental Sciences, University of Sydney, Sydney, NSW, 2006, Australia

ARTICLE INFO

Keywords:
Co-registration
Precision
3D model
Change detection
Photogrammetry

ABSTRACT

Change detection is an essential and widely used approach for investigating ecosystem dynamics. Multi-temporal 3D models increasingly underpin photogrammetry-based analyses of change for many ecologically relevant attributes. To detect change, it is necessary to accurately align 3D models collected at different times using a process referred to as co-registration. However, achieving precise co-registration is difficult in underwater habitats due to practical challenges intrinsic to surveying them. These include a lack of accurate georeferencing information, variable light, turbidity and weather conditions, and diving restrictions dictated by the diver's pressure exposure over time. Here we present an efficient co-registration workflow for 3D models that directly addresses these challenges, derived from underwater structure-from-motion methods. To test our approach, we used 3D models from across a wide range of coral reef habitats covering all those that one may encounter in shallow reefs (15 m depth and above). We then identified and empirically estimated four key sources of error: co-registration, 3D processing, image acquisition, and reference and scaling features (RSF) placement, and quantified their relative contributions to the overall error. Our proposed co-registration workflow had a mean precision of 1.37 ± 16.55 mm. Image acquisition and RSF placement errors contributed the most to the total workflow error (37% and 53%, respectively), while the contribution of co-registration and 3D processing errors was minimal (3% and 7%, respectively). As a result of our analysis, we provide 'good practice' guidelines to reduce errors associated with photogrammetric workflows and to facilitate efficient and reliable detection of 3D change in complex underwater ecosystems.

1. Introduction

Time-series data are essential in ecology (Wauchope et al., 2021). Long-term records of ecological data are used to quantify trends in historical change, characterize habitats, and estimate future responses to environmental change or estimate future conditions (Magurran et al., 2010; Wolfe et al., 1987). In the past two decades, the growing availability of digital photographic sensors such as digital single-lens reflex (DSLR) cameras, along with the development of topographic survey techniques have substantially increased the use of three-dimensional (3D) reconstructions in terrestrial and aquatic ecology (Carrivick and Smith, 2019; Fonstad et al., 2013). The production of high-resolution 3D datasets in time-series sampling regimes has similarly increased, as it enables the characterization of change in 3D structure, and therefore allows more robust detections of temporal change in systems where structural integrity holds importance, such as forests and coral reefs (Graham and Nash, 2013; Shugart et al., 2010). For example, studies aimed at detecting rates of change occurring in the structural properties of key ecological attributes have tracked the gain or loss in 3D structure of habitat engineers (e.g., trees and corals), or shifts in ground or benthic community composition (Burns et al., 2016; Fukunaga et al., 2022; Hardiman et al., 2013; Hernández-Landa et al., 2020; Tompalski et al., 2021).

In recent years, the use of close-range structure-from-motion photogrammetry, hereafter referred to as photogrammetry, has enabled fine spatial scale and high-resolution (0.1–10 mm pixel resolution) topographic reconstructions from overlapping photographs. Model reconstruction techniques applied in photogrammetry utilize paired,

* Corresponding author at: College of Science and Engineering, James Cook University, 1 James Cook Dr, Douglas, QLD 4811, Australia.
E-mail address: marine.lechene@my.jcu.edu.au (M.A.A. Lechene).

https://doi.org/10.1016/j.ecoinf.2024.102632
Received 25 October 2023; Received in revised form 3 May 2024; Accepted 3 May 2024
Available online 5 May 2024

overlapping photographs captured within a network to convert overlapping features into a 3D 'point cloud'. Subsequently, these points are interpolated to generate a series of interconnected triangles which create the 3D model. Scaling and orientation of the resultant 3D products (point cloud or model) is provided by the camera positions and/or by reference and scaling features of known dimensions placed in the scene (Westoby et al., 2012). Three-dimensional photogrammetry products store complex information regarding the surface structure of organisms and environments and thus provide the opportunity to investigate spatio-temporal dynamics of habitats at very fine spatial scales in four dimensions.

To enable detection of fine-scale changes in surveyed surfaces, 3D models must be aligned to a common coordinate system, a process called 'co-registration'. In terrestrial environments, co-registration techniques for land-based 3D products are well established (Dong et al., 2020). These typically use multiple georeferenced point locations obtained by Global Positioning Systems (GPS) (e.g., Coulter and Stow, 2008; Hannam and Moskal, 2015). However, co-registration of underwater 3D models remains a challenge, primarily due to the inability of GPS radio signals to penetrate water (Taraldsen et al., 2011). Moreover, errors in diver-based underwater photogrammetry data can be caused by a range of factors associated with image collection methods in the field. These factors include user-decisions (e.g., camera choice, diver experience, swimming patterns and speed) and environmental conditions (e.g., turbidity, sunlight reflections and shadows) (Bryson et al., 2017; Mangeruga et al., 2018). Any sources of error in co-registration can strongly influence the accuracy and precision of metrics extracted from 3D models, which can ultimately influence their utility for studying environmental change.

Accurate and precise co-registration is particularly essential for multi-temporal analyses of 3D structure dynamics in marine environments such as coral reefs. Typically, establishing mechanically stable reference features to support co-registration is crucial for achieving high accuracy and precision in multi-temporal surveys, but is a significant challenge (Nocerino et al., 2020; Skarlatos et al., 2017). Current methods focus on the installation of physical reference features, which are sometimes extensively developed as a geodetic reference network. Establishing physical features in coral reef environments is typically achieved by drilling and cementing anchors of known coordinates into the reef matrix (e.g., (Kopecky et al., 2023; Neyer et al., 2018; Nocerino et al., 2020; Rossi et al., 2020). These studies highlighted the importance, but also the difficulty, of developing reference features that are stable over time and secured in the reef structure to verify the precision and accuracy of successive 3D models. As a result of these limitations, time-series dynamics of marine environments such as coral reefs have typically been studied at small scales.

An alternative to the physical installation or reference features is the synchronization of underwater cameras with GPS devices floating on the surface (e.g., (Abadie et al., 2018; González-Rivero et al., 2014). This innovative approach allows for the coverage of larger spatial areas (albeit often with a trade-off in image resolution) but is impractical for deep or remote habitats due to challenges diving with tethered instruments. To survey deep ecosystems, it has been necessary to develop workflows that combine a range of sensors, including acoustic sensors and imaging systems, that allow the development of 3D photogrammetric reconstructions from diverse data sources (e.g., Conti et al., 2019).

The use of 3D models in time-series studies within marine environments has been limited primarily due to challenges in the establishment of stable reference features and field data collection. These challenges introduce various errors throughout the process, spanning from initial data collection to the subsequent 3D model processing stages. Although some studies have attempted to quantify the error associated with specific steps of the workflow (Aston et al., 2022; Figueira et al., 2015) and/or to develop a robust geodetic reference system (Marre et al., 2019; Nocerino et al., 2020), they have not addressed all known error sources. Consequently, there is still a clear need to develop new, robust, and scalable techniques for the co-registration of multi-temporal, large-area, high-resolution photogrammetry products.

This study aims to empirically estimate the main errors influencing the precision of an efficient field protocol for multi-temporal analyses of 3D underwater models and provide best practices guidelines to ecologist and conservationists (non-experts in computer vision or photogrammetry) using similar approaches. We used custom designed underwater reference features and efficient co-registration techniques specifically tailored for large-area applications (10s – 100 s of square meters), and the generation of high-resolution, time-series 3D models. To evaluate the repeatability of this protocol, we empirically estimated four key sources of error that can influence the precision of temporal comparison of 3D models: 1) co-registration error, 2) 3D processing error, 3) image acquisition error, and 4) reference and scaling features (RSF) placement error. We present and discuss our findings in the form of 'good practice' guidelines for reliable and effective 3D model change detection using multi-temporal photogrammetry surveys across 10s – 100 s of square meters.

2. Methods

This study was conducted as part of the Ecological Intelligence for Reef Restoration and Adaptation Program (EcoRRAP) (https://gbrrestoration.org/program/ecorrap/). Underwater imagery was collected using EcoRRAP 3D photogrammetry techniques described by Gordon et al. (2023). Study plot setup, field data collection and 3D processing are further detailed in sections 2.2, 2.3 and 2.4 below.

2.1. Sources of error examined

The current study evaluated the total error in a proposed workflow for temporally co-registering underwater 3D models. We partitioned the error focusing on practical units rather than theoretical frameworks to provide actionable guidance for field ecologists. This involved dividing the total error into four key sources: 1) co-registration error, 2) 3D processing error, 3) image acquisition error, and 4) reference and scaling features (RSF) placement error, which were empirically tested (Fig. 1, Table 1). The co-registration error is evaluating the error introduced during the co-registration process. The'3D processing error' refers to the error introduced by the software workflow for Structure-from-Motion using Agisoft Metashape Professional v. 1.8.4 (Agisoft LLC, St. Petersburg, Russia) and with settings detailed in table S2. The 'image acquisition error' refers to the error introduced during the image collection and is specific to the camera network used. All camera settings and processing parameters and statistics are presented in tables S1–3. The 'RSF placement error' is accounting for the precision of placing and replacing reference features consistently between surveys, as well as the impact of scaling features placement throughout the surveyed area. These four sources of error were selected based on expectations that they would be the primary sources of real-world discrepancies that can be mitigated or managed in photogrammetry workflows. While there are many other factors that could influence the precision of temporal data surveys (e.g., environmental conditions; Mangeruga et al., 2018) controlling these variables in the field is challenging and not always possible.

To test the influence of each of the four sources of error, we co-registered the test models (subsequent imaging) with reference models (first imaging) and calculated the model-to-model deviation between the models' surfaces (see section 2.5). In all cases, we used images from contiguous dates (or the same date where available), and similar environmental conditions (i.e., sea state, brightness, time of day, tide height), with no changes in the areas of interest. Ten pairs of models were created, co-registered and compared for each of the four sources of error tested (total of 40 pairs, or 80 models). All 3D models were processed in Agisoft Metashape Professional, hereafter referred to as

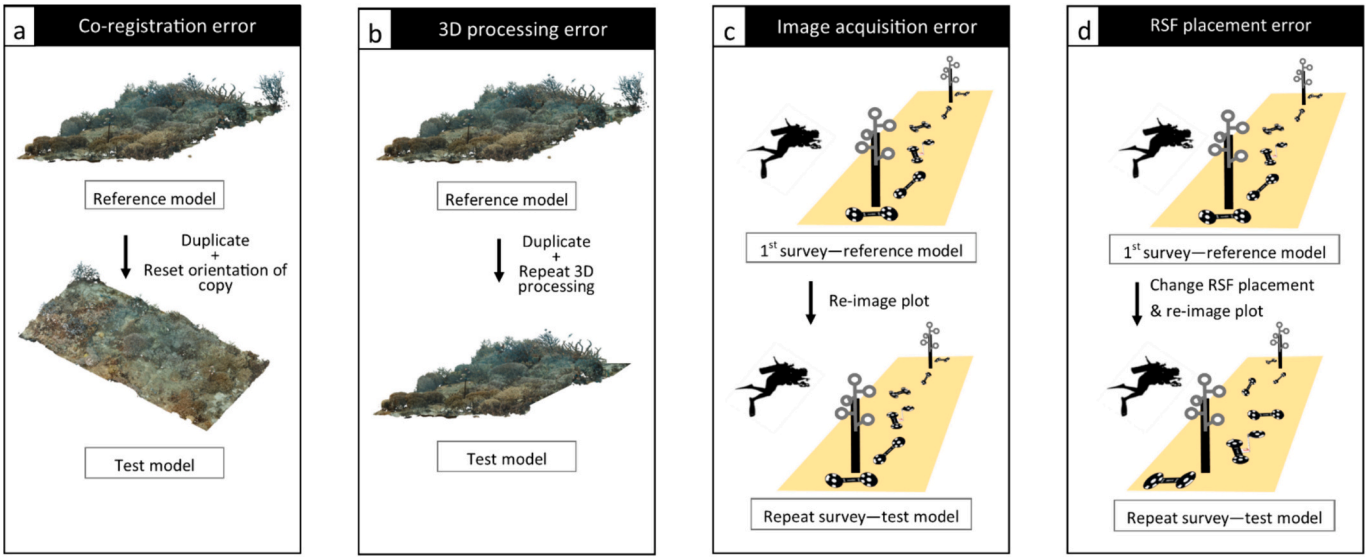

Fig. 1. Conceptual diagram detailing the experimental design around the four sources of error tested in the field and in the office.

Metashape.

2.2. Study plots

Permanent plots (12 × 6 m) were located between 3 and 15 m depth on exposed and sheltered reef slopes and lagoons at multiple reefs on the Great Barrier Reef (GBR). Plots ranged across the most common water visibility conditions found on the GBR (1–20 m vertical visibility). Five stainless steel spheres covered with patterned stickers were mounted on branches to central rod to make sphere-trees references used for plot co-registration (Fig. 3). The top three spheres of each tree were sealed while the two bottom were hollow to achieve near neutral buoyancy underwater. At each permanent plot, two sphere-trees were attached to permanent pickets hammered into the reef substrate along the central line of each plot and roughly 6 m apart. Sphere-trees were mounted on pickets along the small angle of the star-picket, with the second branch (3rd sphere) resting against the top of the picket. The main "trunk" of the sphere-tree was attached against the star picket between its 2nd and the 3rd branches (from the top), using a 3D printed plastic clamp with a T-bolt (Fig. 3). The sphere-trees and clamps were designed in a way that ensured there was only one possible way they could be mounted on the picket, ensuring repeatability from one setup to the next. Additionally, we deployed in each plot six reference features: five 'dumbbell'-shaped features with two coded targets each and one 'triad'-shaped feature with three targets and two bubble-levels (Fig. 4a, c). Coded targets were printed from Metashape. We recorded the depth of one target per feature which was then used in model reconstruction to provide vertical scale and model orientation to real-world up using Metashape.

2.3. Data collection

Photogrammetric surveys of permanent coral reef plots were conducted on SCUBA. Divers used a custom-designed camera platform consisting of two Nikon D850 DSLR cameras with Nikon 20 mm Prime lenses housed in Nauticam underwater housings with 8-in. Nauticam acrylic dome ports. Cameras were mounted 57 cm apart, which ensured

Table 1
The four key sources of error examined in this study, how test models were created, what the inferred error was, and if each of the key sources of error included other sources of error.

Error	Source	Models co-registered	Error inferred	Other error included
Co-registration	Introduced by the co-registration method in CloudCompare	Test models created by duplicating 10 reference models and resetting their orientation at random (i.e., dictated by the position and rotation of the first image taken during the imaging session).	Because each model is co-registered with an exact copy of itself, any model-to-model deviation will be a result of the co-registration step alone (Fig. 1a, Fig. 2).	None
3D processing	Introduced by the stochastic error associated with the reconstruction algorithms in Metashape	Test models created by duplicating 10 photosets used to create reference models and re-processing them using the same reconstruction parameters.	Because each model is processed twice using identical photosets and co-registered with the first version processed, any model-to-model deviation will be a result of the 3D processing and the co-registration steps (Fig. 1b, Fig. 2).	Co-registration
Image acquisition	Introduced by variability in conditions during image acquisition (e.g., swim patterns, camera positions and angles)	Test models created by re-imaging plots consecutively	Because the same plots were imaged consecutively within the same dive, any model-to-model deviation will be a result of the image acquisition, the 3D processing and the co-registration step (Fig. 1c, Fig. 2).	Co-registration, 3D processing
RSF placement	Introduced by the placement of the reference and scaling features in the plot before each imaging	Test models created by re-imaging plots with scaling features moved in different locations within the plot and reference features taken down and put back up	Because the same plots were imaged consecutively but with the reference and scaling features taken down/moved between imaging, the model-to-model deviation will be a result of the image acquisition, the 3D processing, the co-registration and the RSF placement steps (Fig. 1d, Fig. 2).	Co-registration, 3D processing, Image acquisition

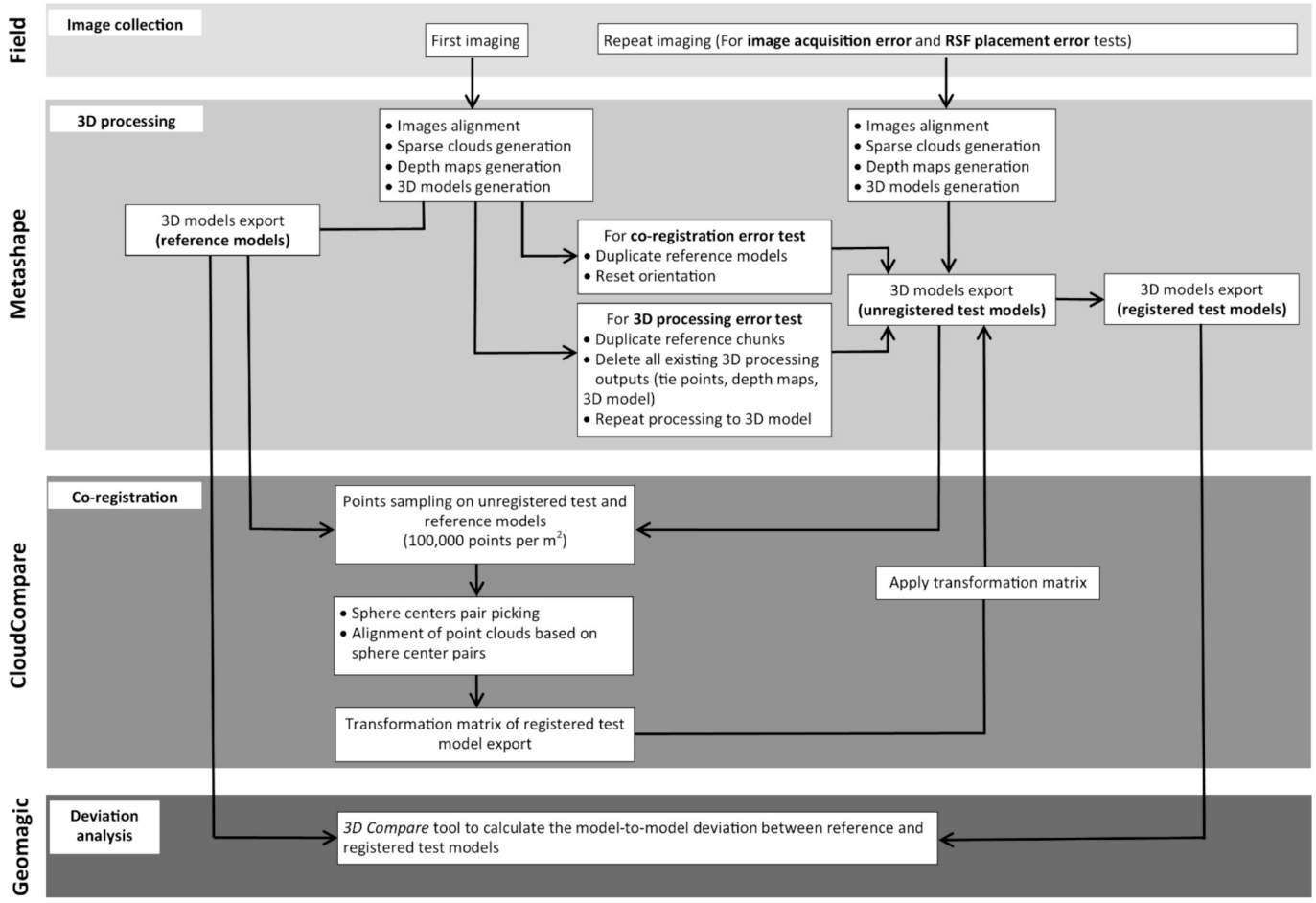

Fig. 2. In- depth workflow diagram detailing all the steps and parameters used from image collection in the field to precision evaluation.

>80% lateral overlap when swimming between 1.5 and 2 m altitude. Images were taken every half a second with settings adjusted to each dive conditions (see Table S1 and Gordon et al., 2023 for camera characteristics and settings details). Image acquisition for the whole plot and sphere-trees was done within the same dive. The diver swam in a 'lawn mower' pattern consisting of five passes in each of the long and short-directions of the plot and swam conical spirals around the sphere-trees at multiple camera angles to achieve accurate reconstruction of all 5 spheres (Fig. 4e).

2.4. 3D processing

Underwater images were processed to generate 3D models in Metashape using custom Python scripts with the parameters detailed in table S2. Reference and unregistered test models were imported into the Open Source software CloudCompare v2.11.3 (Anoia) with default settings. Unregistered test models were co-registered with reference models using the *point-pair picking registration* tool in CloudCompare. By enabling the 'white sphere' icon and setting a search radius, this tool automatically detects the best-fit sphere radius after the user has clicked on the location of the sphere center on the point cloud. Each sphere on the reference model and its equivalent on the test model was selected by clicking on the center of each sphere on the point clouds. The centers of the best-fit sphere were then calculated by the software using a set search radius of 0.05 m because each sphere is 10 cm in diameter. Based on the alignment of the 10 pairs of spheres, CloudCompare then created a transformation matrix for each test model. These matrices were exported and applied to the test model in Metashape via a custom Python script. Once the transformation matrix was applied, both reference and registered test models were exported from Metashape as PLY for model-to-model deviation analysis (Fig. 2).

2.5. Deviation analysis

Each of the four sources of error (Fig. 1) were estimated using the *3D Compare* deviation tool in Geomagic Control X (2020 © 3D Systems) between reference and registered models (Fig. 6). The *3D Compare* deviation tool calculates a deviation value for every (depending on the sampling ratio) vertex of the test model compared to the reference model. Each measured vertex is defined by a set of coordinates (x_{test}, y_{test}, z_{test}) and is associated with a reference set of coordinates of the reference model ($x_{control}$, $y_{control}$, $z_{control}$), which is defined by the projection direction chosen (here we chose the shortest distance). For each point-pair, the tool calculates a gap vector GV defined in Eq. (1).

$$GV = (x_{test} - x_{control}, y_{test} - y_{control}, z_{test} - z_{control}) \quad (1)$$

Where x, y and z correspond to the coordinates on the x, y or z planes of the reference or the test model. GV is then converted to a deviation value between point-pairs D defined in Eq. (2).

$$D = \sqrt{\left(GV_x^2 + GV_y^2 + GV_z^2\right)} \quad (2)$$

For each comparison we reported the arithmetic mean, median, standard deviation (SD) and median absolute deviation (MAD) of all model-to-model deviation (***D***) between models. We report these four statistics because the mean and SD are common descriptive statistics that any user will be familiar with, but they are influenced by extreme values. In this study, the distributions of model-to-model deviations are

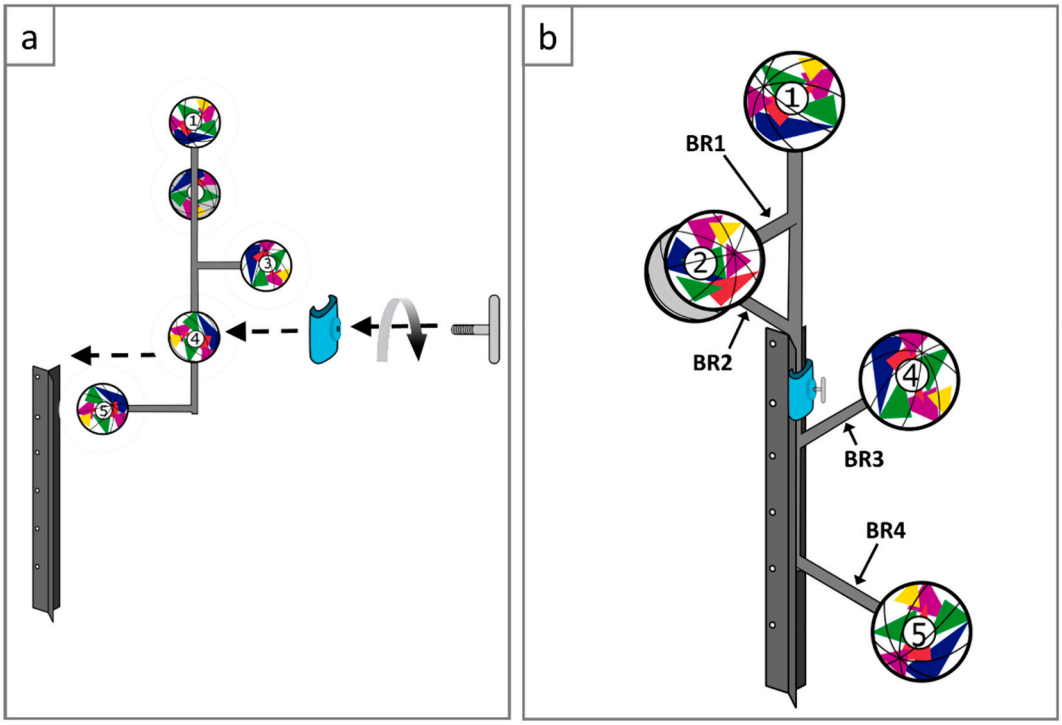

Fig. 3. Design and setup of a sphere-tree. (a) The sphere-tree is mounted on a permanent picket with its second branch resting on top of the picket. It is secured with a plastic clamp and tightened with a T-bolt. (b) A sphere-tree has five spheres covered with patterned stickers and four branches (BR1-BR4) to ensure enough spheres will be well reconstructed and used as co-registration targets.

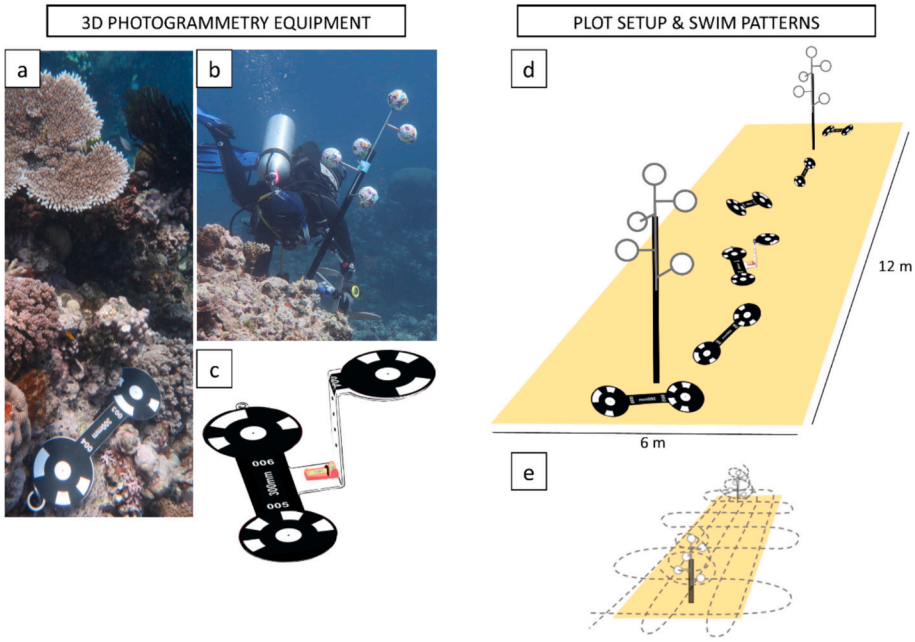

Fig. 4. Diagram of equipment, plot setup and swim patterns used during image acquisition. (a) example of a dumbbell with a pair of Metashape coded-targets used to record depth and scale, (b) example of a sphere-tree on which the co-registration spheres were mounted using a plastic clamp, set on a permanent picket, (c) illustration of a triad comprizing three markers and a spirit level to measure depth and orientation, (d) illustration of a plot setup and (e) swim patterns above the plot and around the sphere-trees during image capture to ensure sufficient overlap between images. Photo credit: K. Fabricius.

expected to be skewed (long tails), even after removing outliers, causing the mean and SD to become biased in some cases. The median and the MAD are more robust to the influence of outliers and long-tails. Instead of using all the point-pairs, we chose a random point-pair sampling ratio of 25% because it represented sufficient data points to observe patterns (22,171,195 to 35,036,902 point-pairs). Outliers' detection was based on model-to-model deviations. Outliers are expected, especially on the edges of the 3D models, as the reconstruction quality can be poor in these areas due to distortion at the edges of photos (Menna et al., 2016) and lower photo overlap caused by the swim patterns (Pizarro et al.,

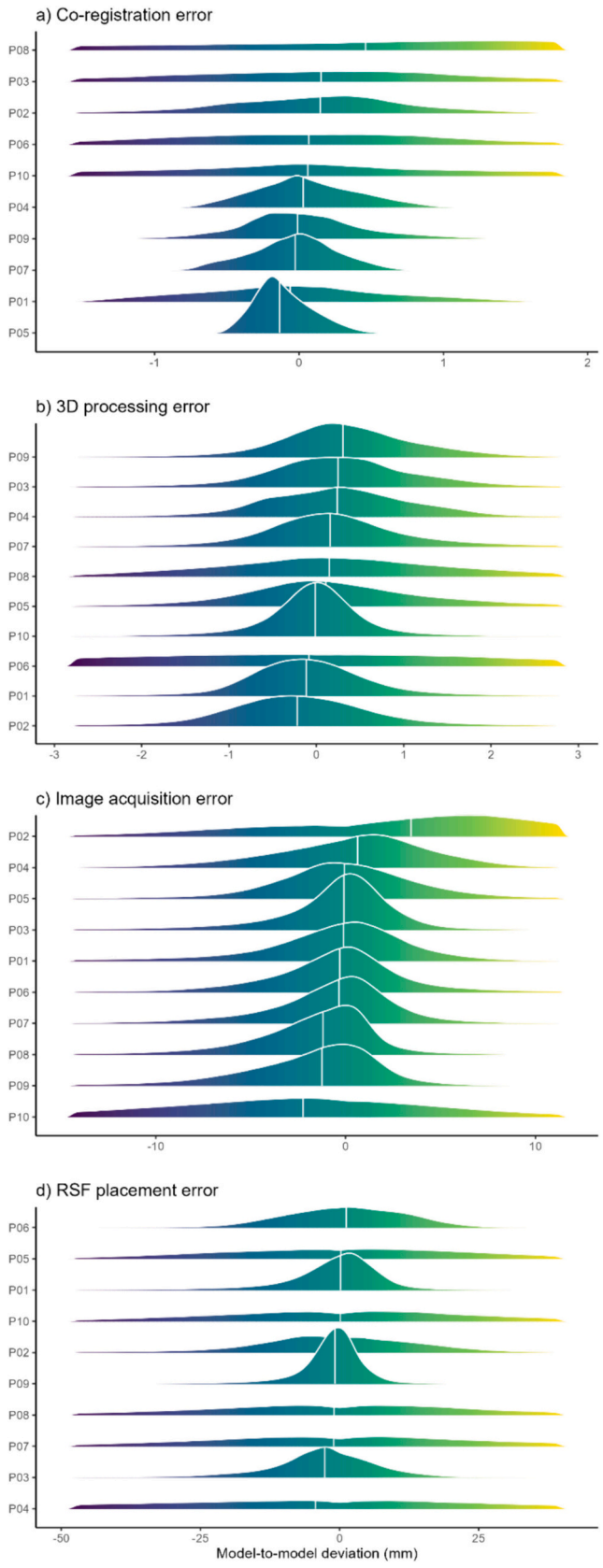

Fig. 5. Distributions of the model-to-model deviations by plots (P01-P10) and source of error (a-d), ranked by model-to-model deviation median values. The white vertical lines correspond to the median of each distribution. Units are in mm. Note that the range along the x-axis is different between sources of error.

2017). Point-pairs with ***D*** falling outside of the 5–95 percentiles were considered as outliers and removed from the dataset for subsequent analyses. We also visually evaluated the spatial distribution of model-to-model deviations between the reference and test models using heatmaps. Distance heatmaps were used to examine if deviations are equally spatially distributed across the models' surfaces.

To gain insight into the distribution of model-to-model deviations within ecologically significant thresholds, we examined the proportion of deviations within specific ranges: −1 to 1 mm, −10 to 10 mm, and −30 to 30 mm. These ranges were selected in accordance with the typical rates of micro change observed in coral reef environments, such as coral growth (~1–60 mm yr^{-1})(Ferrari et al., 2017; Lange et al., 2022), and reef bioerosion (e.g., ~10 mm over a 13-year period)(Roff et al., 2015). Larger changes in the reef 3D structure have been recorded, notably due to mechanical damage from storms or mass coral mortality event (Burns et al., 2016). However, in such instances, the changes observed were at least one order of magnitude greater than the average model-to-model deviations expected to be found in this study; hence, we opted not to incorporate them into our analysis.

The last step was to quantify the contribution of each source of error to the total protocol error. We assumed that errors were additive between each source of error examined because they correspond to independent steps of the protocol. This allowed us to methodically isolate and evaluate the impact of each source of error by sequentially removing them from consideration. This stepwise approach enabled us to approximate the contribution of each step to the overall error based on the absolute mean model-to-model deviations. To calculate the different contributions of each source of error to the overall error, we first calculated each sub-component error by subtracting the error of the previous step. For example, if the mean error associated with the 3D processing step is 0.1, and the 3D processing step also includes the co-registration step that has an error of 0.03, the error introduced by the 3D processing step only is 0.07. We then divided each sub-component mean by the sum of all sub-component means and multiplied it by 100. Knowing the contribution of each step to the overall error allows users to determine where effort should be focused to improve the co-registration workflow.

3. Results

To empirically estimate the main errors influencing the precision of our protocol, we first plotted the distributions of the model-to-model deviations by plots (P01-P10) and source of error (a-d) (Fig. 5). The ranges of deviation values increased from the co-registration error (Fig. 5a) to the RSF placement error (Fig. 5d). The mean model-to-model deviation was 0.038 mm (± 0.602), 0.13 mm (± 0.982), −0.642 mm (± 4.418) and − 1.368 mm (± 16.552) for the co-registration, 3D processing, image acquisition and RSF placement error sources respectively (Table 2). The overall precision of the workflow was 13.4 mm (Table 2, RSF placement error row) for co-registered models derived from independent imaging sessions of the same plot where scale and reference features had been independently placed for each session (Fig. 5, Table 2, RSF placement error row).

The contribution of each source of error to the overall error is presented in Table 2 (% Contribution column). The proportion that each source of error contributed to the overall error was estimated by calculating the absolute mean of each sub-component (source) in a stepwise manner and dividing each sub-component absolute mean by the sum of all sub-component means assuming error is additive between each source. Most of the proposed workflow error can be attributed to two primary sources: 37.43% arises from the image acquisition step, while 53.07% can be attributed to the placement of reference and scaling features (Table 2, % contribution column).

The heatmaps in Fig. 6 are a visual output of the deviation analysis and show the model-to-model deviations between the reference and test models for all the point pairs sampled across the models' surfaces (each

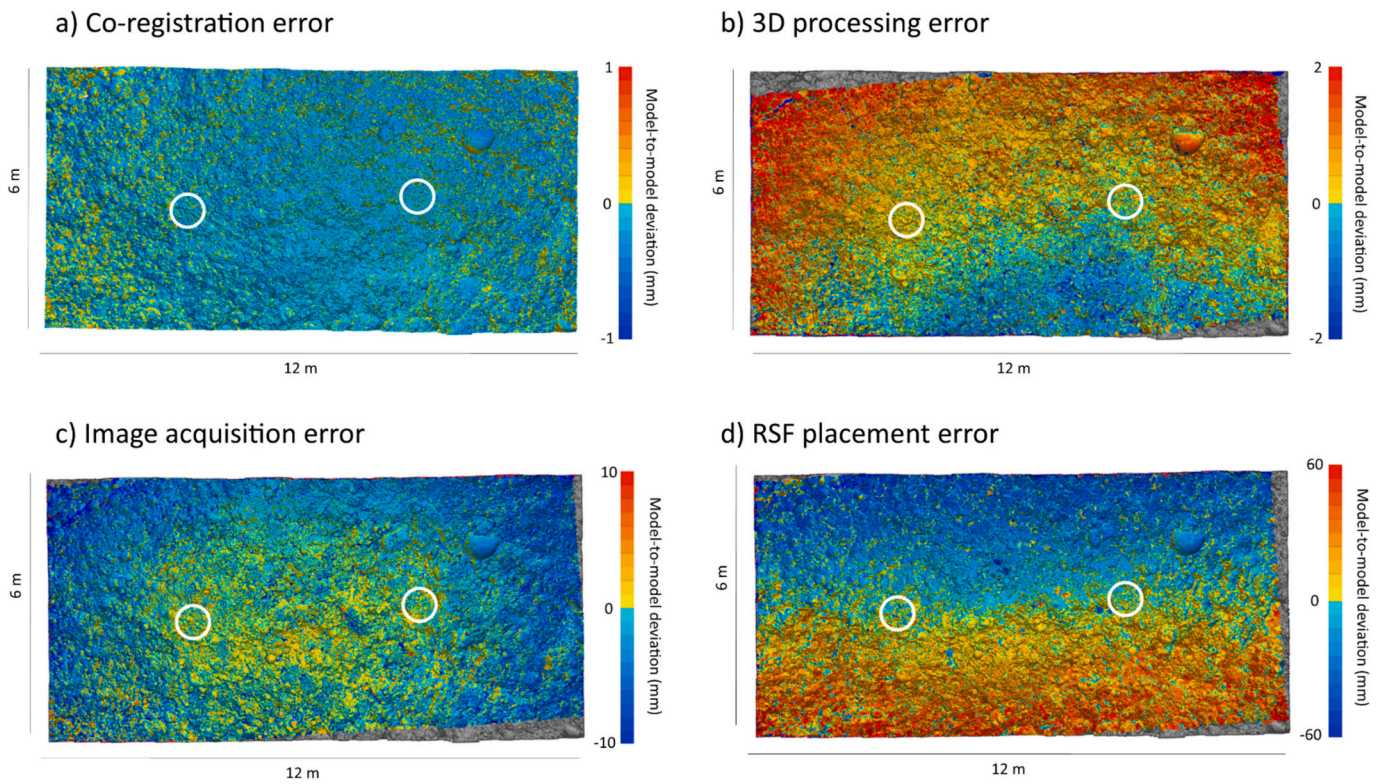

Fig. 6. Example of deviation analysis output using the 3D Compare tool in Geomagic Control X. The heatmaps show the model-to-model deviations (mm) between the reference and test models (note the difference in scale of the heat color ramp). The white circles mark the location of the sphere-trees. Gray areas denote areas of no overlap between models.

colored point represents the deviation, or 3D distance, between a given point on the surface of the reference model and its closest equivalent on the test model's surface). These heatmaps are an efficient visual way of assessing whether the size of the distance between the reference and test models increase with distance from the sphere-trees. They revealed that model-to-model deviations were evenly distributed across the 3D models' surfaces for the co-registration error (Fig. 6a). However, for the three other sources, the smallest deviations tended to be located along the centre line of the plot that correspond to the line between the sphere-trees (prevalence of yellow or light blue points around the centre of the plot) (Fig. 6b-d).

Finally, the proportion of model-to-model deviations within specific ranges are presented in Fig. 7. They revealed that most of the values fell between −1 and 1 mm for the co-registration error (88%) and most values fell between −10 and 10 mm for the 3D processing and image acquisition errors (100% and 96% respectively). However only about half of model-to-model deviations fell between −10 and 10 mm for the RSF placement error, for which 90% of deviations fell between −30 to 30 mm (Table S2, Fig. 7).

4. Discussion

4.1. Context of study

In this study we empirically estimated the main errors influencing the precision of an efficient field protocol for multi-temporal analyses of underwater 3D models. Our analysis revealed that when following the presented protocol, the absolute mean of model-to-model deviation was 1.37 mm and standard deviation of 16.55 mm, meaning that the change detection threshold of this methodology is 33 mm (standard deviation x 2). This suggests that differences greater or lesser than 33 mm at the plot level (across 72 m^2) likely represents a real change in the 3D structure of the reef (Table 2). Thus, the proposed protocol may be sufficient for detecting growth of fast-growing coral taxa (e.g., branching morphologies, Anderson et al., 2017) or the impact of a storm (Pascoe et al., 2021; Yuval et al., 2023), but may not be sufficient for recording slow-growing taxa (e.g., massive morphologies, Cooper et al., 2008) or dissolution of dead corals unless enough time is allowed between surveys to record such changes. The practical and ecological implications of the change detection threshold of the proposed protocol are further discussed in section 4.2 below.

It is important to note that a lower threshold might have been attainable had we based the model-to-model deviation on point-pairs pre-filtered by a confidence interval (James et al., 2017; Lague et al., 2013), instead we used random point-pairs which could encompass bad points (e.g., edges or overhangs). The significance threshold could also have been lowered if we had based our comparisons on cloud-to-cloud or cloud-to-mesh distances (Lague et al., 2013). The decision to use model-to-model comparisons was made however, as 3D models, and not point clouds, are used to derive key habitat metrics in coral reefs such as surface rugosity (Price et al., 2019; Young et al., 2017).

The results presented here are for a single acquisition system (camera, lens and waterproof housing) along with a specific suite of software. The study did not delve into comparing the influence of different camera systems and software on the accuracy of 3D models, as this has been explored in previous research (e.g., Guo et al., 2016; Maas, 2015; Neyer et al., 2018; Rossi et al., 2020). However, it is important to note that both the properties of sea water and the camera system can alter the trajectory of optical rays, thus affecting image formation and quality (Nocerino et al., 2016). Moreover, environmental conditions such as depth, wave action, light reflection, and visibility, can vary strongly and rapidly, impacting image quality (Bryson et al., 2017). To address these factors and ensure comparability, underwater 3D models used in this study were sourced from various regions of the Great Barrier Reef and surveyed around similar times of day and tide levels, representing a typical range of underwater survey conditions. To ensure transparency

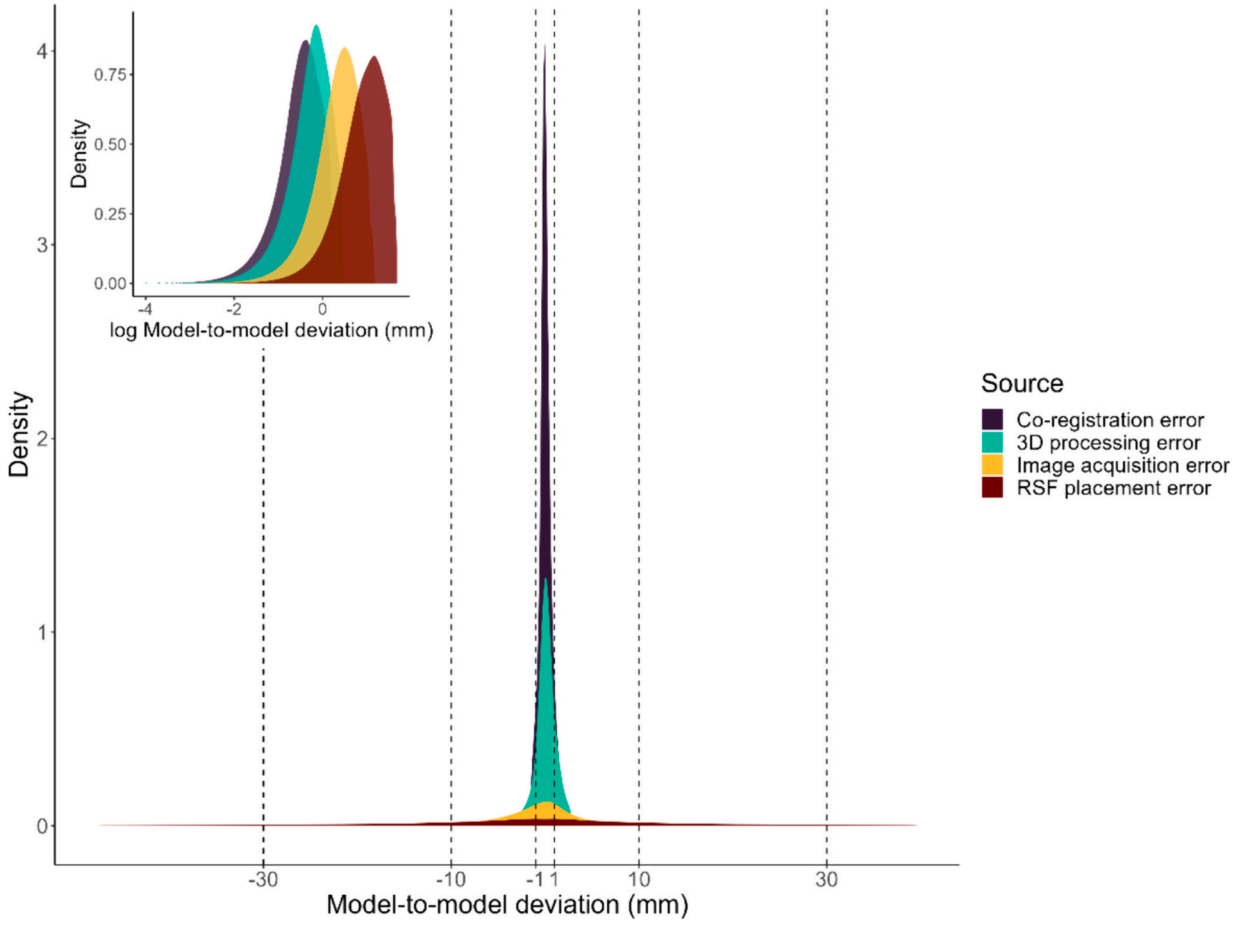

Fig. 7. Distribution of model-to-model deviations. The dashed lines mark the specific ranges evaluated: −1 to 1 mm, −10 to 10, and − 30 to 30 mm. The inset plot shows the model-to-model deviations on a log-transform x-axis for better visualization.

Table 2
Summary statistics (mean, median, standard deviation -SD- and median absolute deviation -MAD-) of model-to-model deviations calculated across all 10 plot pairs for each source of error. The contribution of each source of error to the overall error was estimated by calculating the absolute mean of each sub-component (source) in a stepwise manner and dividing each sub-component absolute mean by the sum of all (1.368), assuming error is additive between each source. For instance, the first row of the % Contribution column was calculated as 0.038/1.368*100. All units are in mm.

Source of error	Mean	Median	SD	MAD	Sub-component absolute mean	% Contribution
Co-registration	0.038	−0.001	0.602	0.495	0.038	2.78
3D processing	0.13	0.111	0.982	0.848	0.092	6.72
Image acquisition	−0.642	−0.357	4.418	3.537	0.512	37.43
RSF placement	−1.368	−0.721	16.552	13.407	0.726	53.07

and reproducibility, camera settings and specific parameters employed during 3D processing in Metashape are detailed in table S2, along with scale bar errors and 3D statistics in table S3.

The mean of the difference between reference and test 3D models, its standard deviation, and mean absolute deviation (based on 10 3D models) for the proposed protocol are −1.34 mm, 16.5 mm and 13.4 mm (Table 2, RSF placement error row). Previous studies have used alternative photogrammetric workflows to detect significant changes in marine environments and found similar error estimates. For example, Neyer et al. (2018), Rossi et al. (2020) and Nocerino et al. (2020) designed and installed a geodetic reference network by cementing anchors into the reef matrix on which ground control points were screwed before imaging. Through use of this installation, they could compare the reconstructions of a reef plot between two epochs (7-months to one year apart). Neyer et al. (2018), found the mean of model-to-model difference, its standard deviation, and the MAD to be 2 mm, 69 mm, and 35 mm respectively for a single plot which are slightly higher than the model-to-model deviation found in the present study based on 10 plots (Table 2, RSF placement error row). Rossi and colleagues compared two models of plots surveyed at a year interval and found the median distance between models to be 12 mm. They concluded that, considering variability introduced by the reconstruction process, only differences greater or lesser than 1 cm per year could be attributed to real change. Furthermore, Nocerino et al. (2020) found significant differences (model-to-model distances) between 50 and − 30 mm corresponding to coral growth and loss that happened within a year.

These alternative workflows consistently delivered precise and accurate repeated measurements of benthic characteristics and change over time. However, the process involves time-consuming steps including the installation, collection of distance measurements and setup of the geodetic reference network within a designated plot, which typically takes two divers and between 1 and 1.5 h to survey an area of ~25 m^2 (Rossi et al., 2020). In contrast, the proposed protocol here requires four divers and between 1 and 1.5 h to survey an area of ~288

m^2 (four plots of 72 m^2 each surveyed per dive). This point is worth considering when scaling up the implementation of the workflow for large scale monitoring. For example, surveying an area of 1000 m^2 would take approximately 40 h with the geodetic network workflow (workflow A) while it would take approximately 3.5 h following the proposed workflow (workflow B). Assuming a maximum of four hours of diving per day is allowed as per most occupational diving restrictions, a 1000 m^2 area would be surveyed in ~10 days with workflow A and in a day or two with workflow B. The proposed workflow has been used to survey annually 360 plots of 72 m^2 each, or a total area of ~25,000 m^2 in 30–45 field days.

The mean absolute error of the workflow presented herein is 1.4 mm (RSF placement error row, Table 2). Assuming that error is additive throughout the steps of the proposed workflow, we could calculate the contribution of each step to the overall error by the co-registration (2.8%), 3D processing (6.7%), image acquisition (37.4%), and RSF placement (53.1%) (Table 2). Although the geodetic reference network-based workflows mentioned earlier require significant labor and time investment, the permanent reference network reduces greatly the primary source of error associated with the method described here (repositioning of the reference and scaling features). Therefore, these two methodologies highlight a trade-off between cost/scale and error.

Knowing the contribution of each step to the overall error provides insight into the factors influencing precision variability between and within surveys, suggesting which step should be modified to achieve the highest precision. Based on these different contributions, we discuss below good practices guidelines to minimize the error associated with each step of the workflow.

4.2. Good practices guidelines for co-registration workflows

The following section discusses the results of the current study in the context of broader applications of multi-temporal photogrammetry surveys. Specifically, we discuss how these findings can inform and shape best practices for multi-temporal imaging when using photogrammetry surveys for assessing ecological indicators.

4.2.1. Establish standard field protocols

The implementation of standard operational procedure within this workflow was crucial and has enabled us to consistently capture images and construct 3D models of the same plots between different epochs and across all common coral reef habitat types between 2 and 15 m depth. The results presented here suggest that efforts should be directed towards implementation of standard protocols to minimize error introduced by the image acquisition step and the placement of reference and scaling features between surveys.

4.2.1.1. Reducing mapping error. The error introduced during the image acquisition step presents a challenge but holds strong potential for improvement. Achieving identical camera angles and positions, even with standardized imaging protocols encompassing factors like swim pattern and speed, remains a challenging task. However, there are several strategies that could be explored to enhance the consistency of data collection.

One strategy to reduce image acquisition error is to maintain the same team of observers over time, although this may be challenging to sustain for long-term monitoring. Alternatively, regular training and calibration among 3D imaging divers can further contribute to minimizing discrepancies. It is important to keep the swim pattern and data collection as consistent as possible while also logistically feasible and safe. For example, Pizarro et al. (2017) proposed a protocol to restrict the swimmer's movement while simultaneously imaging the plot by using a line wound around a drum affixed to a stationary pole. During the image capture, the swimmer unwinds the line resulting in a consistent spiral-like pattern. However, this workflow is best suited for down-looking surveys (only capable of achieving 2.5D, not 3D reconstructions) and would be very challenging to implement safely in most coral reef habitats (reef slopes, lagoons with high structural complexity, in depths >5 m, or in low visibility habitats like inshore reefs). The use of Autonomous Underwater Vehicles (AUVs) could improve image capture patterns in some environments such as deep reef habitats, yet they are significantly more expensive and specialized.

A second strategy to reduce image acquisition error is to increasing image density. Lower density of images can result in less robust 3D reconstruction geometry (James et al., 2017) which could lead to poor co-registration quality. Indeed, in the heatmaps shown in Fig. 6, the model-to-model deviations were smaller around the center line of the plot, potentially due to the higher photo density in this area compared to the edges of the plots. Increasing image density is a viable and easy solution to implement either by swimming slightly slower or by increasing the rate at which images are captured (for example from 1 fps to 2 fps) during image acquisition. Based on our results, if 1.4 mm error is an acceptable threshold, we recommend a minimum image density of 90 images per square meter (~ 6000 images per plot of 72 m^2) which can then be reduced to a third if photo redundancy is high (>2000 images per plot of 72 m^2).

4.2.1.2. Reducing placement of reference and scaling features (RSF) error. The importance and difficulty of setting up permanent references has been repeatedly highlighted by previous studies (e.g., Neyer et al., 2018; Nocerino et al., 2020). We suspect most of the error associated with the reference and scaling features placement is due to permanent pickets moving between imaging sessions or to the sphere-trees moving during imaging sessions, or both. Meticulous attention should be dedicated to the method by which plots are permanently marked and set up for long-term stability. This consideration is particularly crucial in dynamic settings like coral reefs, where external forces have the capacity to alter the positioning of fixed reference points used for co-registration. Introducing as much redundancy as logistically feasible in the number of permanent markers will also help. We found that the reference and scaling feature placement error, accounting for the uncertainty with which the sphere-trees are mounted and re-mounted, had a mean error of 1.37 mm (± 16.5 mm) for an area of 72 sqm. Other stable features, such as rock formations, could be used as additional static references to identify any gross issues with the permanent reference features.

One strategy to reduce RSF error is to improve the design of the permanent markers (the pickets in this study) on which co-registration features (here, sphere-trees) are mounted. While the use of star pickets as permanent anchors offered ease and cost-effectiveness, improving their design could involve shortening their length to reduce susceptibility to hydrodynamic forces (Neyer et al., 2018). The picket's length represents the result of a trade-off between reducing the likelihood of movement and preventing overgrowth by fast-growing benthic organisms. The ideal length of a picket will also depend on the type of substrate at each site, well consolidated reef (typical of shallow exposed reefs) will require shorter pickets, while sites dominated by rubble and weaker substrate (typical of back reefs and lagoons) will require longer pickets. The type of picket should be carefully planned with site knowledge.

The structural integrity of the permanent pickets can also be compromised due to corrosion as we noticed at some of our older plots. Corroded pickets can decrease the mechanical stability of sphere-trees and thus decrease precision of co-registration. Opting for stainless-steel pickets, which are more resistant to corrosion, could present a viable solution, albeit at a higher initial material cost. In this study two pickets per plot were used, offering a little redundancy if one picket moved or corroded. Although our findings indicate that using two pickets leads to an acceptable level of error (Table 2), if logistically and costly feasible, it is worth considering the option of adding a third (forming a triangular arrangement within the plot) or fourth (positioned

in a rhomboid arrangement) permanent picket per plot. This redundancy would safeguard against picket movement or dislodgement and allow each picket to have a sphere-tree with less spheres. Adding a third picket would also reduce the model-to-model distance around the edges of the 3D models as seen in Fig. 6 where the heatmaps showed that error generally increased with distance from the plane along which the pickets were placed.

A second strategy to reduce RSF error is to reduce the probability of co-registration features mounted onto permanent markers to move between or/and during surveys. Notably, we observed that even minor discrepancies in the way sphere-trees were mounted onto the permanent pickets led to a slight increase in model-to-model deviation, and contributed to half the total co-registration error in this study. The use of spheres as co-registration features was very efficient, offering superior alignment capabilities compared to 2D markers or any other published method to the best of our knowledge. To improve setup efficiency, the number of spheres per tree could be reduced from five to two or three (always keep the top sphere) to make sphere-trees less cumbersome and potentially mitigate the impact of water flow forces. Finally, it is also possible to better fix the permanent markers into the seafloor by cementing them for example (Nocerino et al., 2020).

4.2.2. Understand the 3D processing pipeline

Photogrammetry reconstruction software often operates in a black-box mode which may provide unreliable results when users lack a comprehensive understanding of the underlying technique. The error introduced during the 3D processing step using Metashape, a widely used software, was very small (mean model-to-model deviation of 0.13 $\pm$ 0.98 mm). While the task of minimizing reconstruction errors during 3D processing remains challenging, the value of obtaining insights into this error should not be understated. Such insights serve a dual purpose: they aid in compartmentalizing 3D processing error from other potential sources of error, and they provide a quantitative means to gauge the overall precision achieved. Furthermore, quantifying the error introduced during model 3D processing highlights the significant level of change that is detectable using a common processing pipeline in Metashape. We encourage photogrammetry practitioners to either quantify or, at the very least, remain aware of, the error introduced by their 3D processing pipeline, particularly when aiming for very fine change detection (mm scale).

4.2.3. Survey at relevant frequency

The results provide insights into the appropriate temporal frequency for sampling, emphasizing that this frequency should be informed by the rate of change in the measured variables and the error associated with the sampling protocol. Based on our results, sampling should be conducted when at least $\pm$30 mm of change is likely to have occurred over an area of 72 m^2 (Fig. 7, Table S4). The main application for which precise co-registration is needed at the plot level is to detect changes in the 3D structural complexity over time. The 3D structural complexity of ecosystems, often created or enhanced by ecosystem engineers such as corals and trees, has a profound effect on communities of associated organisms (Graham and Nash, 2013; Romero et al., 2015). Thus, structural complexity metrics are often used as proxies for ecosystem state and resilience in coral reefs (Cheung et al., 2021; Yuval et al., 2023). There are many processes, such as storms (Madin and Connolly, 2006), coral predator outbreaks (Kayal et al., 2012), and mass bleaching (Hughes et al., 2018), that can change the 3D structure of reefs. The threshold presented here can be used as a distance cut-off when comparing models of different time points such as in Yuval et al. (2023) that used a distance cut-off of 0.05 m to reliably quantify change related to the impact of a storm on a reef.

The workflow proposed in this study was not exclusively designed for detecting very fine changes such as those occurring at the organism level in 3D (e.g., coral colony growth); although the detection of such fine changes was a significant aspect under investigation. If one's primary interest lies in coral growth for instance, an optimal imaging approach would involve individual colony imaging (i.e., creating 3D models of individual coral colonies not of whole plots). Our workflow was strategically developed to facilitate the comprehensive monitoring of various critical facets of coral reef recovery and adaptation. These aspects encompassed demography, landscape ecology, structural complexity, seascape genomics, fish shelter space availability, and spatial distribution of corallivory and herbivory, among others, across spatial extents of 100 s of square meters. However, for practitioners intending to utilize this dataset for demography, a secondary fine alignment of 3D models should complement the proposed workflow. For instance, studying the growth of slow-growing coral such as massive coral morphologies, which extend at $<$20 mm yr^{-1} (Cooper et al., 2008; Roff and Mumby, 2012) would require a secondary fine alignment and enough time between surveys to detect real changes.

4.2.4. Important considerations

The findings presented herein are tailored to the specific camera network, calibration parameters and suite of software used. While the outlined good practices guidelines aspire for universal applicability across similar workflows, it is important to acknowledge that using different cameras, calibration parameters, or software packages for 3D model processing will result in differences in uncertainty stemming from both random and systematic errors particular to the camera network and settings used. For instance, the use of auto-focus camera settings while the camera-to-object distance varies during image capture can result in images with different focal lengths being used to compute a unique model with a constant focal length (Ricolfe-Viala and Esparza, 2021). Consequently, this computed model may not accurately reflect the true camera location during the capture of calibration images, potentially impacting the accuracy of the resulting 3D model. Although the cumulative error encompassing random and systematic errors affecting the 3D models was captured within the overall error evaluation in this study, quantifying their individual contribution lay beyond the scope of this study.

Finally, the principal limitation identified in this study pertains to the mechanical stability of reference features. Notably, even a slight shift of one of the sphere-trees led to alignment discrepancies, as highlighted in Fig. 6d. This underscores the main limitation of using target-based co-registration in highly dynamic environments such as coral reefs. Therefore, our results indicate that future users could refine the co-registration method presented here by using approaches that consider the full geometry of 3D models, rather than relying solely on external features.

5. Conclusion

The accuracy and precision of co-registration play a pivotal role in the reliability of metric comparisons, particularly when assessing changes between time points. Precise measurements between these time points are essential because they provide the capability to determine how reefs are either accreting or eroding over time. Small errors in multi-temporal surveys and co-registration can lead to misleading interpretations, making it imperative to ensure precise survey methods and 3D models' alignment for a more robust understanding of the dynamic processes shaping reef 3D structure.

This study expands upon prior research using thorough and precise but time-consuming methodologies, proposing a complementary workflow that offers a cost-effective and time-efficient approach on a larger scale with similar error. We expect our experimental approach to estimating multi-temporal survey error can reduce a broad range of common error sources in photogrammetric analyses to improve precision. Importantly, as sources of error begin to be controlled, the value of time-series imagery data increases, and will ultimately support long-term, ultra-fine resolution, and precise studies of environmental change.

CRediT authorship contribution statement

Marine A.A. Lechene: Writing – review & editing, Writing – original draft, Visualization, Validation, Methodology, Formal analysis, Conceptualization. **Will F. Figueira:** Writing – review & editing, Supervision, Methodology, Conceptualization. **Nicholas J. Murray:** Writing – review & editing, Supervision. **Eoghan A. Aston:** Writing – review & editing, Methodology. **Sophie E. Gordon:** Writing – review & editing, Methodology, Data curation. **Renata Ferrari:** Writing – review & editing, Supervision, Methodology, Formal analysis, Conceptualization.

Declaration of competing interest

The authors declare that they have no known competing financial interests or personal relationships that could have appeared to influence the work reported in this paper.

Data availability

The Python scripts mentioned for 3D processing are openly available on the GitHub repository at https://github.com/open-AIMS/EcoRRAP/tree/main/Metashape%20processing. Data will be made available on request.

Acknowledgement

The authors thank Januar Harianto and Zal Khambatta Cowasji for their help at the inception of this project. This work was supported by the Reef Restoration and Adaptation Program, funded by the partnership between the Australian Government's Reef Trust and the Great Barrier Reef Foundation. The conclusions drawn here are those of the authors and do not reflect the broader views of the Reef Restoration and Adaptation Program.

Appendix A. Supplementary data

Supplementary data to this article can be found online at https://doi.org/10.1016/j.ecoinf.2024.102632.

References

Abadie, A., Boissery, P., Christophe, V., 2018. Georeferenced underwater photogrammetry to map marine habitats and submerged artificial structures. Photogramm. Rec. 33, 448–469. https://doi.org/10.1111/phor.12263.

Anderson, K.D., Cantin, N.E., Heron, S.F., Pisapia, C., Pratchett, M.S., 2017. Variation in growth rates of branching corals along Australia's great barrier reef. Sci. Rep. 7 (1), 2920. https://doi.org/10.1038/s41598-017-03085-1.

Aston, E.A., Duce, S., Hoey, A.S., Ferrari, R., 2022. A protocol for extracting structural metrics from 3D reconstructions of corals. Front. Mar. Sci. 9 https://doi.org/10.3389/fmars.2022.854395.

Bryson, M., Ferrari, R., Figueira, W., Pizarro, O., Madin, J., Williams, S., Byrne, M., 2017. Characterization of measurement errors using structure-from-motion and photogrammetry to measure marine habitat structural complexity. Ecol. Evol. 7 (15), 5669–5681. https://doi.org/10.1002/ece3.3127.

Burns, J.H.R., Delparte, D., Kapono, L., Belt, M., Gates, R.D., Takabayashi, M., 2016. Assessing the impact of acute disturbances on the structure and composition of a coral community using innovative 3D reconstruction techniques. Methods Oceanogr. 15–16, 49–59. https://doi.org/10.1016/j.mio.2016.04.001.

Carrivick, J.L., Smith, M.W., 2019. Fluvial and aquatic applications of structure from motion photogrammetry and unmanned aerial vehicle/drone technology. WIREs Water 6 (1), e1328. https://doi.org/10.1002/wat2.1328.

Cheung, P.-Y., Nozawa, Y., Miki, T., 2021. Ecosystem engineering structures facilitate ecological resilience: A coral reef model. Ecol. Res. 36 (4), 673–685. https://doi.org/10.1111/1440-1703.12230.

Conti, L.A., Lim, A., Wheeler, A.J., 2019. High resolution mapping of a cold water coral mound. Sci. Rep. 9 (1) https://doi.org/10.1038/s41598-018-37725-x. Article 1.

Cooper, T.F., De'ath, G., Fabricius, K.E., Lough, J.M., 2008. Declining coral calcification in massive Porites in two nearshore regions of the northern great barrier reef. Glob. Chang. Biol. 14 (3), 529–538. https://doi.org/10.1111/j.1365-2486.2007.01520.x.

Coulter, L., Stow, D., 2008. Assessment of the spatial co-registration of multitemporal imagery from large format digital cameras in the context of detailed change detection. Sensors 8 (4), 2161–2173. https://doi.org/10.3390/s8042161.

Dong, Z., Liang, F., Yang, B., Xu, Y., Zang, Y., Li, J., Wang, Y., Dai, W., Fan, H., Hyyppä, J., Stilla, U., 2020. Registration of large-scale terrestrial laser scanner point clouds: A review and benchmark. ISPRS J. Photogramm. Remote Sens. 163, 327–342. https://doi.org/10.1016/j.isprsjprs.2020.03.013.

Ferrari, R., Figueira, W.F., Pratchett, M.S., Boube, T., Adam, A., Kobelkowsky-Vidrio, T., Doo, S.S., Atwood, T.B., Byrne, M., 2017. 3D photogrammetry quantifies growth and external erosion of individual coral colonies and skeletons. Sci. Rep. 7 (1), 16737. https://doi.org/10.1038/s41598-017-16408-z.

Figueira, W., Ferrari, R., Weatherby, E., Porter, A., Hawes, S., Byrne, M., 2015. Accuracy and precision of habitat structural complexity metrics derived from underwater photogrammetry. Remote Sens. 7 (12), 16883–16900. https://doi.org/10.3390/rs71215859.

Fonstad, M.A., Dietrich, J.T., Courville, B.C., Jensen, J.L., Carbonneau, P.E., 2013. Topographic structure from motion: A new development in photogrammetric measurement. Earth Surf. Process. Landf. 38 (4), 421–430. https://doi.org/10.1002/esp.3366.

Fukunaga, A., Pascoe, K.H., Pugh, A.R., Kosaki, R.K., Burns, J.H.R., 2022. Underwater photogrammetry captures the initial recovery of a coral reef at Lalo atoll. Diversity 14 (1). https://doi.org/10.3390/d14010039. Article 1.

González-Rivero, M., Bongaerts, P., Beijbom, O., Pizarro, O., Friedman, A., Rodriguez-Ramirez, A., Upcroft, B., Laffoley, D., Kline, D., Bailhache, C., Vevers, R., Hoegh-Guldberg, O., 2014. The Catlin Seaview survey – kilometre-scale seascape assessment, and monitoring of coral reef ecosystems. Aquat. Conserv. Mar. Freshwat. Ecosyst. 24 (S2), 184–198. https://doi.org/10.1002/aqc.2505.

Gordon, S., Aston, E., Lechene, M., Harianto, J., Figueira, W., Gonzalez Rivero, M., Ferrari, R., 2023. Field photogrammetry in 4D. Reef restoration and adaption program (EcoRRAP). In: Standard Operational Procedure Number 1: Overview and in-field workflow. https://doi.org/10.25845/SE7T-PS86.

Graham, N.A.J., Nash, K.L., 2013. The importance of structural complexity in coral reef ecosystems. Coral Reefs 32 (2), 315–326. https://doi.org/10.1007/s00338-012-0984-y.

Guo, T., Capra, A., Troyer, M., Grün, A., Brooks, A.J., Hench, J.L., Schmitt, R.J., Holbrook, S.J., Dubbini, M., 2016. Accuracy Assessment of Underwater Photogrammetric Three Dimensional Modelling for Coral Reefs [Application/Pdf]. https://doi.org/10.3929/ETHZ-B-000118990.

Hannam, M., Moskal, L.M., 2015. Terrestrial laser scanning reveals seagrass microhabitat structure on a tideflat. Remote Sens. 7 (3) https://doi.org/10.3390/rs70303037. Article 3.

Hardiman, B.S., Gough, C.M., Halperin, A., Hofmeister, K.L., Nave, L.E., Bohrer, G., Curtis, P.S., 2013. Maintaining high rates of carbon storage in old forests: A mechanism linking canopy structure to forest function. For. Ecol. Manag. 298, 111–119. https://doi.org/10.1016/j.foreco.2013.02.031.

Hernández-Landa, R.C., Barrera-Falcon, E., Rioja-Nieto, R., 2020. Size-frequency distribution of coral assemblages in insular shallow reefs of the Mexican Caribbean using underwater photogrammetry. PeerJ 8, e8957. https://doi.org/10.7717/peerj.8957.

Hughes, T.P., Kerry, J.T., Baird, A.H., Connolly, S.R., Dietzel, A., Eakin, C.M., Heron, S.F., Hoey, A.S., Hoogenboom, M.O., Liu, G., McWilliam, M.J., Pears, R.J., Pratchett, M.S., Skirving, W.J., Stella, J.S., Torda, G., 2018. Global warming transforms coral reef assemblages. Nature 556 (7702), 492–496. https://doi.org/10.1038/s41586-018-0041-2.

James, M.R., Robson, S., d'Oleire-Oltmanns, S., Niethammer, U., 2017. Optimising UAV topographic surveys processed with structure-from-motion: ground control quality, quantity and bundle adjustment. Geomorphology 280, 51–66. https://doi.org/10.1016/j.geomorph.2016.11.021.

Kayal, M., Vercelloni, J., de Loma, T.L., Bosserelle, P., Chancerelle, Y., Geoffroy, S., Stievenart, C., Michonneau, F., Penin, L., Planes, S., Adjeroud, M., 2012. Predator crown-of-thorns starfish (Acanthaster planci) outbreak, mass mortality of corals, and cascading effects on reef fish and benthic communities. PLoS One 7 (10), e47363. https://doi.org/10.1371/journal.pone.0047363.

Kopecky, K.L., Pavoni, G., Nocerino, E., Brooks, A.J., Corsini, M., Menna, F., Gallagher, J. P., Capra, A., Castagnetti, C., Rossi, P., Gruen, A., Neyer, F., Muntoni, A., Ponchio, F., Cignoni, P., Troyer, M., Holbrook, S.J., Schmitt, R.J., 2023. Quantifying the loss of coral from a bleaching event using underwater photogrammetry and AI-assisted image segmentation. Remote Sens. 15 (16) https://doi.org/10.3390/rs15164077. Article 16.

Lague, D., Brodu, N., Leroux, J., 2013. Accurate 3D comparison of complex topography with terrestrial laser scanner: application to the Rangitikei canyon (N-Z). ISPRS J. Photogramm. Remote Sens. 82, 10–26. https://doi.org/10.1016/j.isprsjprs.2013.04.009.

Lange, I.D., Molina-Hernández, A., Medellín-Maldonado, F., Perry, C.T., Álvarez-Filip, L., 2022. Structure-from-motion photogrammetry demonstrates variability in coral growth within colonies and across habitats. PLoS One 17 (11), e0277546. https://doi.org/10.1371/journal.pone.0277546.

Maas, H.-G., 2015. On the accuracy potential in underwater/multimedia photogrammetry. Sensors 15 (8). https://doi.org/10.3390/s150818140. Article 8.

Madin, J.S., Connolly, S.R., 2006. Ecological consequences of major hydrodynamic disturbances on coral reefs. Nature 444 (7118), 477–480. https://doi.org/10.1038/nature05328.

Magurran, A.E., Baillie, S.R., Buckland, S.T., Dick, J. McP, Elston, D.A., Scott, E.M., Smith, R.I., Somerfield, P.J., Watt, A.D., 2010. Long-term datasets in biodiversity research and monitoring: assessing change in ecological communities through time. Trends Ecol. Evol. 25 (10), 574–582. https://doi.org/10.1016/j.tree.2010.06.016.

Mangeruga, M., Bruno, F., Cozza, M., Agrafiotis, P., Skarlatos, D., 2018. Guidelines for underwater image enhancement based on benchmarking of different methods. Remote Sens. 10 (10) https://doi.org/10.3390/rs10101652. Article 10.

Marre, G., Holon, F., Luque, S., Boissery, P., Deter, J., 2019. Monitoring marine habitats with photogrammetry: A cost-effective, accurate, precise and high-resolution reconstruction method. Front. Mar. Sci. 6, 276. https://doi.org/10.3389/fmars.2019.00276.

Menna, F., Nocerino, E., Fassi, F., Remondino, F., 2016. Geometric and optic characterization of a hemispherical dome port for underwater photogrammetry. Sensors 16 (1). https://doi.org/10.3390/s16010048. Article 1.

Neyer, F., Nocerino, E., Gruen, A., 2018. Monitoring coral growth—The dichotomy between underwater photogrammetry and geodetic control network. Int. Arch. Photogramm. Remote. Sens. Spat. Inf. Sci. XLII–2, 759–766. https://doi.org/10.5194/isprs-archives-XLII-2-759-2018.

Nocerino, E., Menna, F., Fassi, F., Remondino, F., 2016. Underwater calibration of dome port pressure housings. ISPRS - Int. Arch. Photogrammet. Remote Sens. Spatial Inform. Sci. XL-3 (W4), 127–134. https://doi.org/10.5194/isprsarchives-XL-3-W4-127-2016.

Nocerino, E., Menna, F., Gruen, A., Troyer, M., Capra, A., Castagnetti, C., Rossi, P., Brooks, A.J., Schmitt, R.J., Holbrook, S.J., 2020. Coral reef monitoring by scuba divers using underwater photogrammetry and geodetic surveying. Remote Sens. 12 (18) https://doi.org/10.3390/rs12183036. Article 18.

Pascoe, K.H., Fukunaga, A., Kosaki, R.K., Burns, J.H.R., 2021. 3D assessment of a coral reef at Lalo atoll reveals varying responses of habitat metrics following a catastrophic hurricane. Sci. Rep. 11 (1), 12050. https://doi.org/10.1038/s41598-021-91509-4.

Pizarro, O., Friedman, A., Bryson, M., Williams, S.B., Madin, J., 2017. A simple, fast, and repeatable survey method for underwater visual 3D benthic mapping and monitoring. Ecol. Evol. 7 (6), 1770–1782. https://doi.org/10.1002/ece3.2701.

Price, D.M., Robert, K., Callaway, A., Lo Lacono, C., Hall, R.A., Huvenne, V.A.I., 2019. Using 3D photogrammetry from ROV video to quantify cold-water coral reef structural complexity and investigate its influence on biodiversity and community assemblage. Coral Reefs 38 (5), 1007–1021. https://doi.org/10.1007/s00338-019-01827-3.

Ricolfe-Viala, C., Esparza, A., 2021. The influence of autofocus lenses in the camera calibration process. IEEE Trans. Instrum. Meas. 70, 1–15. https://doi.org/10.1109/TIM.2021.3055793.

Roff, G., Mumby, P.J., 2012. Global disparity in the resilience of coral reefs. Trends Ecol. Evol. 27 (7), 404–413. https://doi.org/10.1016/j.tree.2012.04.007.

Roff, G., Zhao, J., Mumby, P.J., 2015. Decadal-scale rates of reef erosion following El Niño-related mass coral mortality. Glob. Chang. Biol. 21 (12), 4415–4424. https://doi.org/10.1111/gcb.13006.

Romero, G.Q., Gonçalves-Souza, T., Vieira, C., Koricheva, J., 2015. Ecosystem engineering effects on species diversity across ecosystems: A meta-analysis. Biol. Rev. 90 (3), 877–890. https://doi.org/10.1111/brv.12138.

Rossi, P., Castagnetti, C., Capra, A., Brooks, A.J., Mancini, F., 2020. Detecting change in coral reef 3D structure using underwater photogrammetry: critical issues and performance metrics. Appl. Geomat. 12 (S1), 3–17. https://doi.org/10.1007/s12518-019-00263-w.

Shugart, H.H., Saatchi, S., Hall, F.G., 2010. Importance of structure and its measurement in quantifying function of forest ecosystems. J. Geophys. Res. Biogeosci. 115 (G2) https://doi.org/10.1029/2009JG000993.

Skarlatos, D., Agrafiotis, P., Menna, F., Nocerino, E., Remondino, F., 2017. Ground Control Networks for Underwater Photogrammetry in Archaeological Excavations.

Taraldsen, G., Reinen, T., Berg, T., 2011. The underwater GPS problem. In: OCEANS 2011 IEEE - Spain, p. 8. https://doi.org/10.1109/Oceans-Spain.2011.6003649.

Tompalski, P., Coops, N.C., White, J.C., Goodbody, T.R.H., Hennigar, C.R., Wulder, M.A., Socha, J., Woods, M.E., 2021. Estimating changes in Forest attributes and enhancing growth projections: A review of existing approaches and future directions using airborne 3D point cloud data. Curr. For. Rep. 7 (1), 1–24. https://doi.org/10.1007/s40725-021-00135-w.

Wauchope, H.S., Amano, T., Geldmann, J., Johnston, A., Simmons, B.I., Sutherland, W.J., Jones, J.P.G., 2021. Evaluating impact using time-series data. Trends Ecol. Evol. 36 (3), 196–205. https://doi.org/10.1016/j.tree.2020.11.001.

Westoby, M.J., Brasington, J., Glasser, N.F., Hambrey, M.J., Reynolds, J.M., 2012. 'Structure-from-Motion' photogrammetry: A low-cost, effective tool for geoscience applications. Geomorphology 179, 300–314. https://doi.org/10.1016/j.geomorph.2012.08.021.

Wolfe, D.A., Champ, M.A., Flemer, D.A., Mearns, A.J., 1987. Long-term biological data sets: their role in research, monitoring, and management of estuarine and coastal marine systems. Estuaries 10 (3), 181–193. https://doi.org/10.2307/1351847.

Young, G.C., Dey, S., Rogers, A.D., Exton, D., 2017. Cost and time-effective method for multi-scale measures of rugosity, fractal dimension, and vector dispersion from coral reef 3D models. PLoS One 12 (4), e0175341. https://doi.org/10.1371/journal.pone.0175341.

Yuval, M., Pearl, N., Tchernov, D., Martinez, S., Loya, Y., Bar-Massada, A., Treibitz, T., 2023. Assessment of storm impact on coral reef structural complexity. Sci. Total Environ. 891, 164493 https://doi.org/10.1016/j.scitotenv.2023.164493.